# Preparation and Adsorption of $CO_2$ and $H_2$ by Activated Carbon Hollow Fibers from Rubber Wood (*Hevea brasiliensis*)

Liyan Ma,[a,b] Jianing Li,*[,a] and Xiaojun Ma *

A series of activated carbon hollow fibers doped with charcoal powder (WC-ACHFs) were prepared from wood waste with great potential for application in the gas adsorption of $CO_2$ and $H_2$. The hydrogen storage of WC-ACHF-1.0% increased approximately 10.5% more than that of activated carbon hollow fibers (ACHF), and the highest hydrogen uptake reached 4.51 wt% at 77 K and 100 bar. Regarding the $CO_2$ adsorption, the highest adsorption amount reached 7.13 mmol $g^{-1}$ and the mass content was 31.35 at 273 K, which was 49.8% higher than the sample without doping. In addition, the multiple heteroatoms (N, P) from wood waste liquefaction had a synergistic effect on the gas adsorption properties of WC-ACHFs. These results showed that a facile method was promising for the preparation of wood-derived activated carbon hollow fibers from forestry and agricultural residues in the application of gas adsorption.

*Keywords: Wood waste; Activated carbon fibers; Hydrogen storage; $CO_2$ adsorption*

*Contact information: a: Ministry of Agriculture Key Laboratory of Biology and Genetic Resource Utilization of Rubber Tree/State Key Laboratory Breeding Base of Cultivation & Physiology for Tropical Crops, Rubber Research Institute, Chinese Academy of Tropical Agricultural Sciences, Danzhou 571737, China; b: Department of Wood Science and Technology, Tianjin University of Science & Technology, Tianjin 300222, China; *Corresponding author: ljn206@163.com;mxj75@tust.edu.cn*

## INTRODUCTION

With the continuous consumption of fossil energy, global carbon emissions have dramatically increased, resulting in the greenhouse effect, haze, and other environmental hazards. The development of carbon capture and storage (CCS) technologies, as well as sustainable, efficient, and clean energy sources and carriers, including supercapacitors, hydrogen storage and bioenergy, has become extremely urgent (Chen *et al.* 2019).

Porous carbon materials have been proposed for a long time as promising $CO_2$ and $H_2$ adsorbents, which is due to their light weight, high specific surface area, complete reversibility, low cost, and availability (Ramesh *et al.* 2015; Sangeetha and Selvakumar 2018). For $CO_2$ adsorption, the increase of specific surface area, the highly porous structure, and the enhancement of the interaction between the gas and carbon material by doping heteroatom are of great importance for the adsorption of carbon materials. However, regarding the hydrogen storage, under weak van der Waals forces, narrower pores result in stronger hydrogen molecules-to-surface interactions, and higher heat of the adsorption and the adsorption capacity. Both theoretical studies and experimental research have suggested that 0.6-nm-wide pore size is ideal for hydrogen storage at 77 K due to the overlap of potential fields from the pore walls on both sides (Ramesh *et al.* 2015; Sethia and Sayari 2016). Hence, ultramicropore carbon materials have important significance in hydrogen storage due to their enhanced adsorption heat (Huang *et al.* 2018a).

Activated carbon hollow fibers (ACHF) are a kind of non-crystalline porous carbon obtained by the pyrolysis of carbon materials. Carbon generates more pores and changes its volume, shape, and size through activation steps (Wróbel-Iwaniec *et al.* 2015). Oxidizing gases react preferentially with amorphous carbon and carbon at lattice defects in the carbide during physical activation. Carbon is burned out, volatilized, and etched continuously, and the pores are thus formed, thereby increasing the pore structure of the activated carbon (Huang and Zhao 2016; Bader and Ouederni 2017). Therefore, some researchers have studied one-dimensional wood-based carbon fibers with controllable carbonaceous architecture and pore size distribution as gas adsorption materials.

In this work, the authors studied a facile approach to fabricate activated carbon hollow fibers doped with charcoal powder (WC-ACHFs) from rubber wood waste *via* liquefaction, melt spinning, and steam activation methods. The effects of wood charcoal on the morphology, the specific surface area, the structure, and the composition of ACHF were investigated. This work exhibits a pathway to design economic and sustainable gas adsorption materials from forestry and agricultural residues.

## EXPERIMENTAL

### Materials

Rubber wood (*Hevea brasiliensis*) waste was supplied by a wood furniture factory (Tianjin Dongsheng Furniture Co., Ltd, Tianjin, China). Commercial wood charcoal powder (WC) was purchased from Donghai Carbon Corporation, Tianjin, China. Phenol, hexamethylenetetramine, hydrochloric acid (HCl, 37.9 wt% in water), formaldehyde ($CH_2O$, 37.9 wt% in water), methanol ($CH_3OH$, 99.9 wt% in water) and phosphoric acid ($H_3PO_4$, 37.9 wt% in water) were purchased from Tianjin Fengchuan Chemical Reagent Technology Co., Ltd. (Tianjin, China). All chemicals were supplied as analytical grade and were used without further purification.

*Preparation of activated carbon fibers with hollow structure by doping with charcoal powder*

The ACHF was prepared from rubber wood. First, 20 g of wood (0.2 < diameter of particle < 0.8 mm), 120 g of phenol, as well as 9.6 g of $H_3PO_4$ were mixed in a certain proportion and heated with stirring from room temperature to 160 °C to prepare wood liquefaction through oil bath reaction (at 160 °C for 2 h). Then, the different proportions of charcoal powder (0.5 wt%, 1 wt%, 2 wt%, and 3wt%, based on wood liquefaction) were added to the mixed solution of wood liquefaction and 10 wt% hexamethylenetetramine (on the weight of liquefaction solution) to prepare the spinning solution. The primary fibers were further obtained through melt spinning. The primary fibers were semi-cured in a mixture solution of 18.95% HCl and 18.95% $CH_2O$. Then, the semi-cured fibers were dipped into 18.95% methanol solution at 50 °C for 1 h. Subsequently, the semi-cured fibers were dipped into the same solution described in the first step to obtain the hollow fibers. The five groups of hollow fibers were placed in a tube furnace. Under the protection of the flow rate of 100 mL/min $N_2$, the heating rate at 5 °C/min was uniformly heated to the set activation temperature (800 °C), held isothermally for 1 h at a steam flow of 10 g/min, and after that cooled to 25 °C to obtain the activated carbon hollow fibers doped with charcoal powder (Scheme 1).

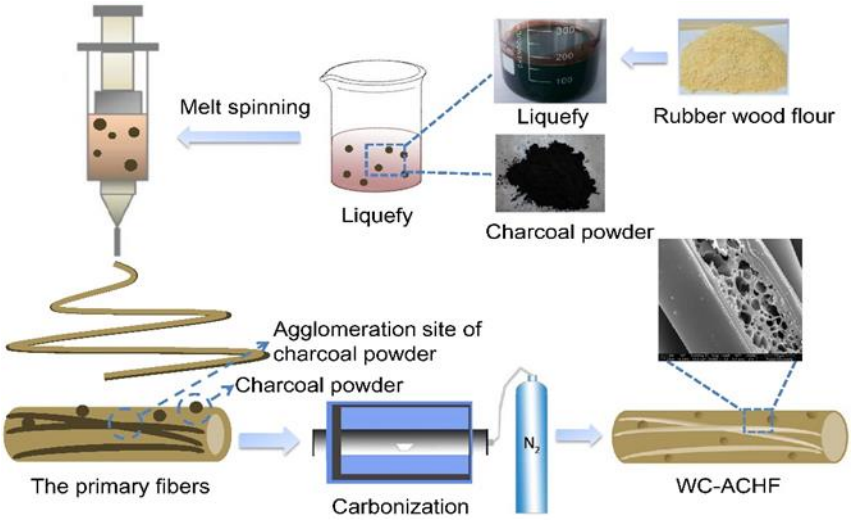


**Scheme 1.** Schematic illustration of WC-ACHFs fabrication

## Methods

The morphology and energy dispersive spectroscopy (EDS) mapping were obtained *via* scanning electron microscopy (SEM, model SU1510; Hitachi, Tokyo, Japan).

The surface analysis was achieved through a Kratos Axis UltraDLD multi-technique X-ray photoelectron spectrometer (XPS) (ESCALAB 250Xi; Thermo Fisher Scientific Inc., Waltham, MA, USA).

The $N_2$ adsorption–desorption isotherms, the surface area, and the porosity of the samples were obtained at 77 K using an ASAP 2020 automatic apparatus (Micromeritics Instrument Co., Norcross, GA, USA). The micropore area (Smicro) and micropore volume (Vmicro) were obtained by the t-plot method. The mesopore area (Smeso) and mesopore volume (Vmeso) were calculated by the Barrett–Joyner–Halenda method.

Hydrogen adsorption and desorption studies were obtained in the pressure ranges 0 to 100 bar and at 77 K using a high-pressure Automated Sievert's apparatus from Advanced Material Corporation, Norcross, GA, USA (Ramesh *et al.* 2015).

The $CO_2$ adsorption analysis was measured at 273 K, and the adsorption isotherms were determined by dosing $CO_2$ volumes of 0.2 standard temperature and pressure (STP) $cm^3\ g^{-1}$ up to a $P/P_0$ of $10^{-4}$, a $P/P_0$ table was used to construct the $CO_2$ adsorption isotherm up to a final $P/P_0$ of 1.

# RESULTS AND DISCUSSION

## Morphology and Compositions

The morphology of the WC-ACHFs was observed using SEM, as shown in Fig. 1. Compared with the ACHF (Fig. 1a), the WC-ACHFs (Fig. 1b) exhibited abundant pore structure, and the surface of WC-ACHF-1.0% displayed a large amount of pores. This was due to the formation of a large number of agglomerated charcoal particles in the wall of ACHF, resulting in the formation of an ACHF surface that was not compact and the doping of charcoal powder with the main ingredient of carbon element provided more active sites for activation reaction as well as formed more pores during activation reaction involving the following several steps (1 through 3) (Fig. 1c). Therefore, the concentration range of

charcoal powder used in this study had a remarkable effect on the surface morphology. In addition, the WC-ACHFs showed a rich porous structure on the inner and outer surface of the hollow fibers, which greatly increased its specific surface area. The EDX spectrum analysis indicated that some heteroatoms of O, N, and P were well-distributed in various samples, which may have been derived from chemical substances, such as hexamethylenetetramine and phosphoric acid, during wood liquefaction (Ma *et al.* 2014; Barman and Nanda 2018).

$$C + H_2O \rightarrow H_2 + CO \quad (1)$$

$$CO + 2H_2O \rightarrow 2H_2 + CO_2 \quad (2)$$

$$C + CO_2 \rightarrow 2CO \quad (3)$$

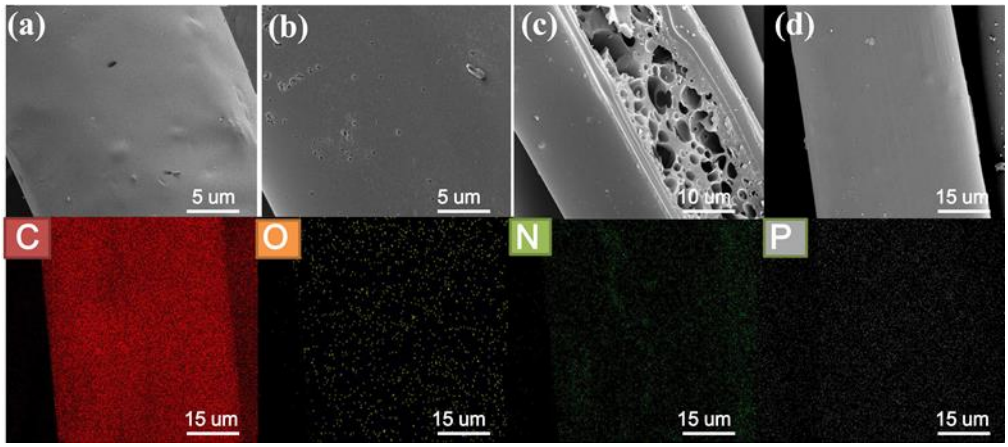


**Fig. 1.** (a) SEM image of ACHF; (b), (c), and (d) SEM images of WC-ACHF-1%; bottom row is the EDX spectra of fig.1d

The XPS of the prepared WC-ACHF samples, shown in Fig. 2a, clearly indicated the existence of C, N, O, and P in the sample. The C1s signals of all WC-ACHF samples exhibited an asymmetric tailing, which was the contribution of the intrinsic asymmetry of the graphite peaks (Fig. 2b) and an increase in the relative content of carbon bonded to oxygen-containing functions after the increasing of charcoal powder proportion (Table 1) (Kostoglou *et al.* 2017). The N1s spectrum (Fig. 2c) shows peaks at binding energies 396.41, 399.8, and 405.4 eV corresponding to nitride or aromatic amine, imide, and pyridine-nitrogen-oxide, respectively (Yang *et al.* 2019). The deconvolution of the O1s region spectrum (Fig. 2d) produced three groups of peaks at 530.8 eV, 532.1 eV, and 533.7 eV (Zhou *et al.* 2018). These peaks correspond to hydroxyl, carbonyl oxygen in amide, and carboxyl (Huang *et al.* 2018b; Guo *et al.* 2019). According to relevant reports that the multiple heteroatoms (N, O, and P) from wood liquefaction have a synergistic effect on hydrogen storage properties of ACHF, the existence of polar molecules is conducive to enhancing the chemisorption ability of nitrogen (He *et al.* 2018; Jeong *et al.* 2019). Nitrogen doping was beneficial to the adsorption of hydrogen at low pressure, but a higher nitrogen content at high pressure was not conducive to the adsorption of hydrogen. This was because nitrogen doping reduced the interaction between the hydrogen and pore structure of the samples, thereby affecting the overall nitrogen adsorption capacity of the material (Sethia and Sayari 2016). The hydrogen storage of WC-ACHF-3.0% with a nitrogen content of 1.04% (compared with WC-ACHF-0%, WC-ACHF-0.5%, WC-ACHF-

1.0%, and WC-ACHF-2.0% with nitrogen contents of 0%, 0.77%, 1.06%, and 0.79%, respectively) at high pressure was affected by these factors.

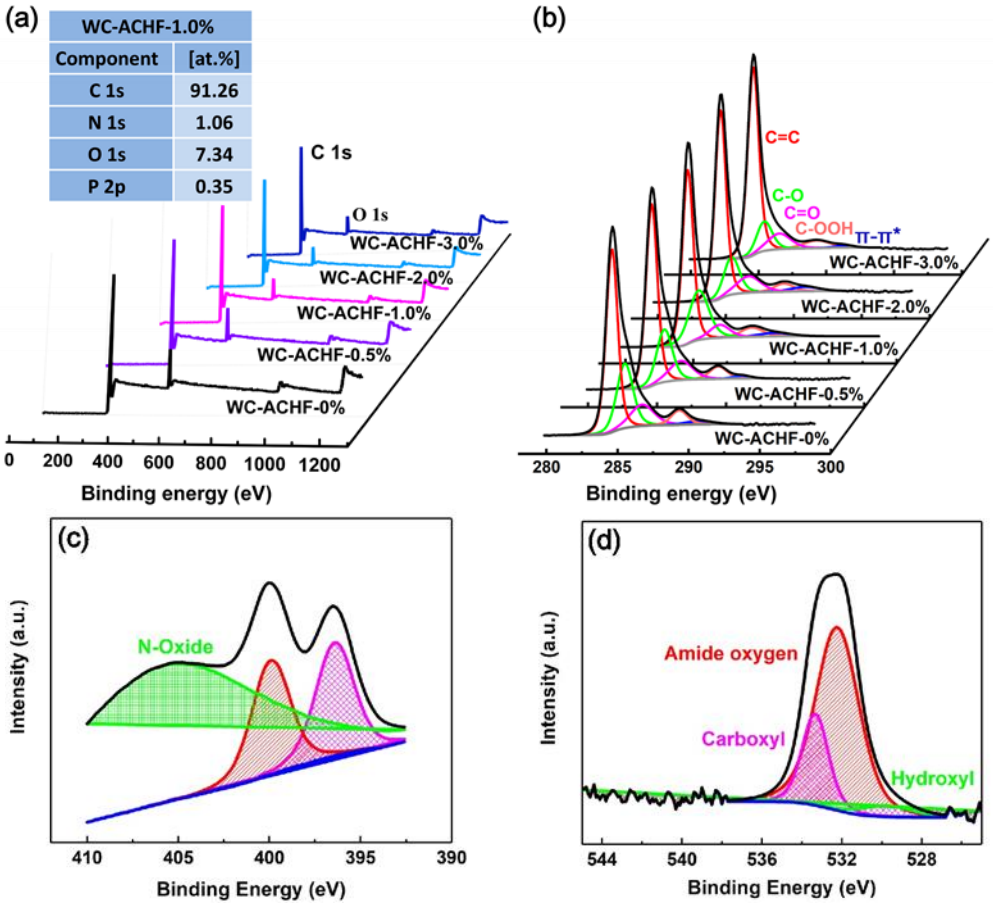


**Fig. 2.** XPS spectra of WC-ACHF: (a) XPS analysis on all elements; (b) XPS analysis on C1s of WC-ACHFs; (c) XPS analysis on N1s; and (d) XPS analysis on O1s

**Table 1.** Results of the C1s Regions, Values Given in % of Total Intensity

| Samples | *Graphite* | | *C-O* | | *C=O* | | *C-OOH* | | $CO_3^{2-}$,*CO*,$CO_2$ | |
|---|---|---|---|---|---|---|---|---|---|---|
| | *BE (eV)* | *M (%)* | *BE (eV)* | *M (%)* | *BE (eV)* | *M (%)* | *BE (eV)* | *M (%)* | *BE (eV)* | *M (%)* |
| WC-ACHF-0% | 284.6 | 64.5 | 285.5 | 22.3 | 286.7 | 7.4 | 289.3 | 5.8 | 290.7 | 2.2 |
| WC-ACHF-0.5% | 284.6 | 53.3 | 285.5 | 25.9 | 286.7 | 12.6 | 289.3 | 5.8 | 290.7 | 2.2 |
| WC-ACHF-1.0% | 284.6 | 54.6 | 285.5 | 26.4 | 286.7 | 12.6 | 289.3 | 5.8 | 290.7 | 2.2 |
| WC-ACHF-2.0% | 284.6 | 57.5 | 285.5 | 22.6 | 286.7 | 12.4 | 289.4 | 5.9 | 291.1 | 1.4 |
| WC-ACHF-3.0% | 284.6 | 62.3 | 285.5 | 22.6 | 286.7 | 12.4 | 289.4 | 5.9 | 291.1 | 1.4 |

All of the WC-ACHF samples possessed the ultramicroporosity (< 0.7 nm), and the maximum pore volume was distributed from 0.5 to 1 nm (Sawant *et al.* 2017). Clearly, WC-ACHF-1.0% with uniform ultramicroporosity possessed a higher pore volume compared with the others. The specific surface area and total pore volume of the WC-ACHF-1.0% reached a maximum at 1902 $m^2$ $g^{-1}$ and 0.860 $cm^3$ $g^{-1}$, which was attributed to the agglomeration of charcoal powder in the spinning solution and the less compact surface of ACHF produced by the spinning step, which provided more reaction sites for activation reaction and formed an abundant amount of pores on the wall of the ACHF. Nevertheless, the excessive increase of the content of charcoal powder and the decreased specific surface area (Fig. 3) was due to excessive charcoal powder adsorbing free $^{+}CH_2OH$, preventing the reaction of liquefied products with it from forming a network structure. This caused the primary fibers to become more compact and to exhibit pore-forming difficulty during activation reaction.

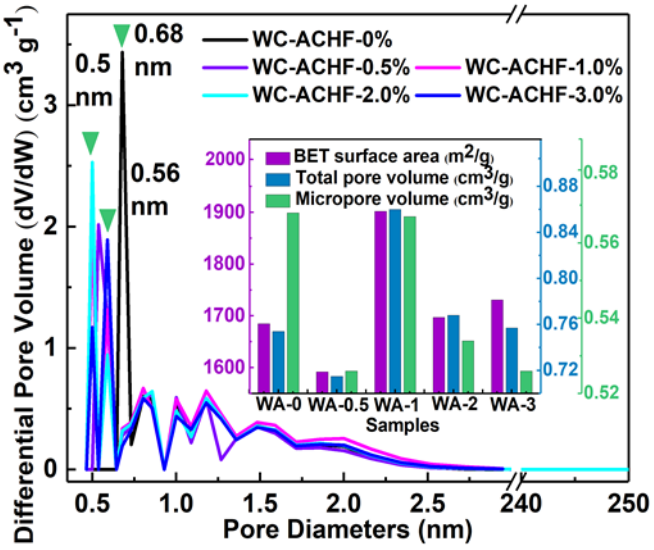


**Fig. 3.** Pore size distribution curves of all series (inset: Pore structure parameters of activated carbon hollow fibers)

## Hydrogen Adsorption Performance

Figure 4a shows the hydrogen adsorption isotherms of all samples at 77 K and 1 bar pressure, which showed that the hydrogen adsorption was entirely reversible. The inset figure summarizes the $H_2$ storage capacities of all sample materials, which shows the $H_2$ storage ranging from 2.06 to 2.24 wt% at 77 K and 1 bar. These results were competitive with those of the recently reported hydrogen adsorbents fabricated on activated carbon (1.4 to 1.97wt% at 77 K and 1 bar) (Arshad *et al.* 2016; Rambau *et al.* 2018). Figure 4b exhibits the adsorption storage of hydrogen of all samples at 77 K and pressures from 0 to 100 bar with various charcoal powder proportions. The inset figure exhibits the $H_2$ adsorption storage ranging from 4.08 to 4.51 wt% at 77 K and 100 bar. With an increased charcoal powder content, the hydrogen storage first increased and then decreased. The hydrogen storage capacity of WC-ACHF-1.0% was the highest, which was roughly the same as that of Fig. 4a. In addition, the hydrogen storage capacities at 77 K and 100 bar were investigated with respect to several textural properties. The obtained ACHF data indicated that the micropore volume, specific surface area, and total pore

volume had no remarkable effect on the hydrogen absorption at high and low pressure (Fig. 4c through 4e). Even at high pressure the hydrogen storage capacity was less than WA-0.5. As reported in a previous study (Lee *et al*. 2017), this revealed that the hydrogen adsorption storage was not completely based on the pore volume and specific surface area. This indicated that pore size distribution played an important role in determining the hydrogen adsorption performance of the carbon fibers. The porosity of WC-ACHFs was mainly composed of two sets of ultramicropores with diameters of 0.50 and 0.56 nm (Fig. 3), and the porosity of ACHF was mainly 0.68 nm ultramicropores. In the samples prepared, WA-1.0 had the highest hydrogen storage capacity, which was attributed to the large ultramicropore volume from the pore size centered at 0.56 nm. Both theoretical studies and experimental results indicated that the pore size width of 0.56 nm was suitable for hydrogen adsorption storage (Sethia and Sayari 2016).

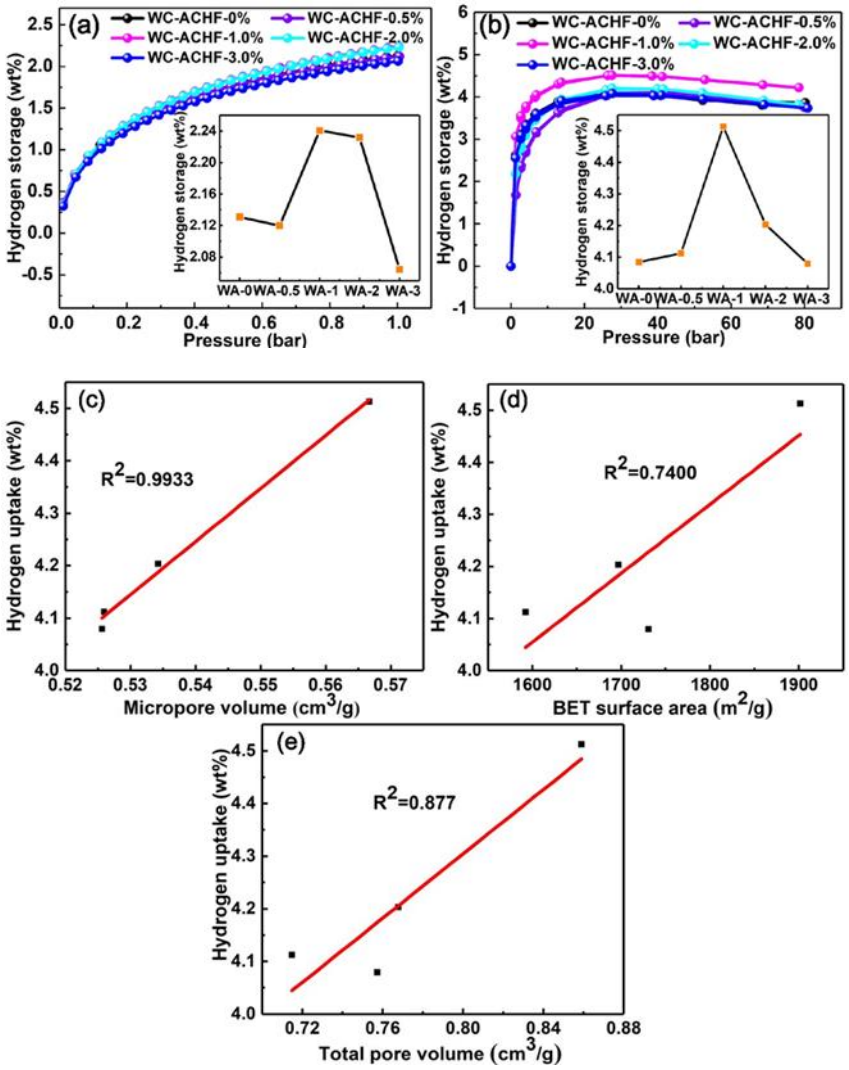


**Fig. 4.** (a) 77 K/$H_2$ adsorption isotherms at 1 bar; (b) 77 K/$H_2$ adsorption isotherms at 100 bar; (c) through (e) The fitting curves of micropore volume, specific surface area, total pore volume, and hydrogen storage of WC-ACHFs at 77 K and 100 bar

Under weak van der Waals forces, narrower pores resulted in stronger hydrogen molecules-to-surface interactions, higher heat of the adsorption and the adsorption capacity, and hence shows a great remarkable influence on the hydrogen adsorption storage of the carbon fibers (Sevilla and Mokaya 2014; Sethia and Sayari 2016). With the enlargement of the pore size, the interaction energy and hydrogen uptake decreased.

## $CO_2$ Adsorption Performance

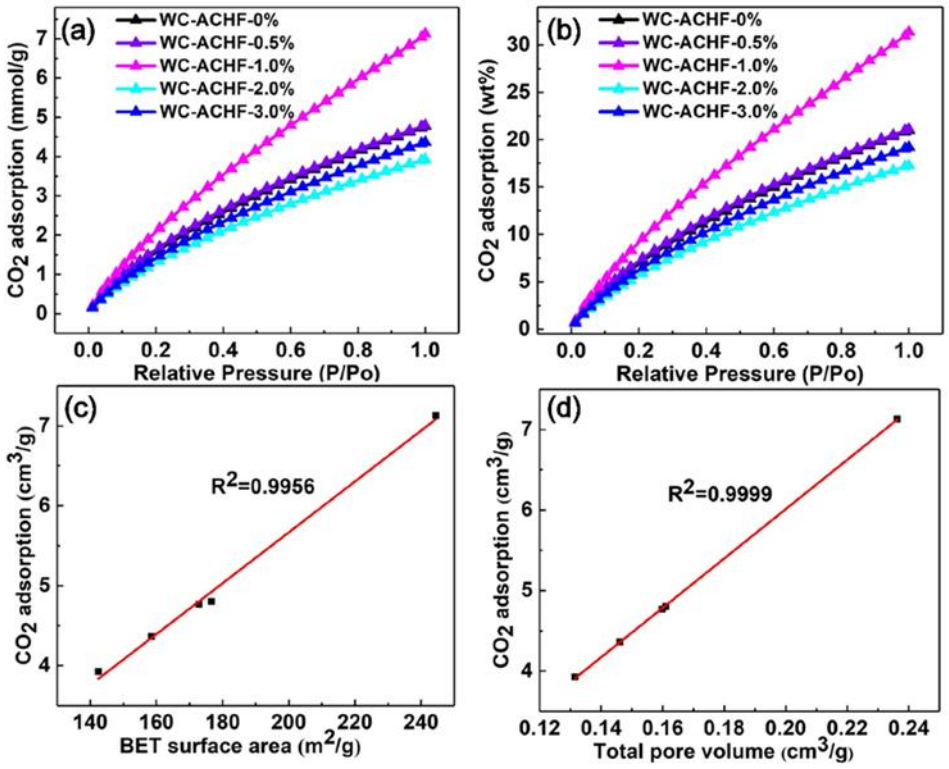


**Fig. 5.** (a) and (b): $CO_2$ sorption isotherms of WC-ACHFs at 273 K; (c) and (d) the fitting curves of specific surface area, total pore volume, and hydrogen storage of WC-ACHFs at 273 K

The $CO_2$ adsorption isotherms of WC-ACHF-0%, WC-ACHF-0.5%, WC-ACHF-1.0%, WC-ACHF-2.0%, and WC-ACHF-3% at 273 K are depicted in Figs. 5a through 5b. The isotherms exhibit the uptake of 4.76, 4.80, 7.13, 3.93, and 4.36 mmol $g^{-1}$. The corresponding mass content was 20.97 wt%, 21.12 wt%, 31.35 wt%, 17.28 wt%, and 19.20 wt%, which is competitive with those of the recently reported $CO_2$ adsorbents fabricated on activated carbon (5.8 mmol $g^{-1}$ at 273 K) (Sreńscek-Nazzal and Kiełbasa 2019). The superior performance of the $CO_2$ absorption of WC-ACHFs compared to the hydrogen absorption was attributed to $CO_2$ being a polar molecule that interacted easily with functional groups on the surface of carbon fibers (as described in the XPS analysis). With the increase in the charcoal powder content, the $CO_2$ adsorption first increased and then decreased. The fitting curves of the specific surface area, total pore volume, and $CO_2$ adsorption of WC-ACHFs at 273 K were further studied (Fig. 5c through 5d). The obtained WC-ACHFs data indicated that specific surface area and total pore volume had a noticeable effect on

$CO_2$ adsorption at 273 K, and revealed that a larger specific surface area and pore volume were more conducive to $CO_2$ adsorption. The adsorption curve of $CO_2$ was different from that of hydrogen, not only because the kinetic diameter of $CO_2$ (0.33 nm) was larger than that of hydrogen (0.289 nm), but also the selective adsorption of WC-ACHFs for different gases there was a difference. For example, the polar groups on the surface of WC-ACHFs can adsorb polar molecule carbon dioxide rather than non-polar molecule hydrogen through van der Waals force (Li *et al.* 2016). In addition, the adsorption amount and heat of $CO_2$ decreased with the increase in pore size, which was consistent with the analysis of hydrogen adsorption (Cao *et al.* 2019). Thus, the addition of the charcoal powder was an effective approach to improve the $CO_2$ adsorption enthalpy.

## CONCLUSIONS

1. A series of wood-derived WC-ACHFs were prepared from rubber wood (*Hevea brasiliensis*) waste through liquefaction, half-curing, melt spinning, and steam activation methods.
2. The optimized carbon material WC-ACHF-1.0% had a high surface area of approximately 1902 $m^2$ $g^{-1}$ and a large volume of ultramicropores centered at 0.56 nm in size. It displayed a hydrogen storage of 4.51 wt% at 298 K and 100 bar, and the $CO_2$ adsorption amount reached 7.13 mol $g^{-1}$ at 273 K.
3. Sustainable wood-derived carbon fibers from forestry and agricultural residues are promising candidates as adsorption gas materials.

## ACKNOWLEDGMENTS

This research was financially supported by the Opening Project Fund of the Key Laboratory of Biology and Genetic Resources of Rubber Tree, the Ministry of Agriculture and Rural Affairs, the P. R. China/State Key Laboratory Breeding Base of Cultivation & Physiology for Tropical Crops/Danzhou Investigation & Experiment Station of Tropical Crops, the Ministry of Agriculture and Rural Affairs, the P. R. China (RRI-KLOF201801), and the National Natural Science Foundation of China (Grant Nos. 31870564, 31270607, and 30901133).

## REFERENCES CITED

Arshad, S. H. M., Ngadi, N., and Aziz, A. A. (2016). "Preparation of activated carbon from empty fruit bunch for hydrogen storage," *J. Energ. Chem.* 8, 257-261. DOI: 10.1016/j.est.2016.10.001

Bader, N., and Ouederni, A. (2017). "Functionalized and metal-doped biomass-derived activated carbons for energy storage application," *Journal of Energy Storage* 13, 268-276. DOI: 10.1016/j.est.2017.07.013

Barman, B. K., and Nanda, K. K. (2018). "CoFe nanoalloys encapsulated in N-doped graphene layers as a Pt-free multifunctional robust catalyst: Elucidating the role of

co-alloying and N-doping," *ACS Sustain. Chem. Eng.* 6(10), 12736-12745. DOI: 10.1021/acssuschemeng.8b01861

Cao, S., Li, B., Zhu, R., and Pang, H. (2019). "Design and synthesis of covalent organic frameworks towards energy and environment fields," *Chem. Eng. J.* 355, 602-623. DOI: 10.1016/j.cej.2018.08.184

Chen, G., Lei, T., Wang, Z., Liu, S., He, X., Guan, Q., Xin, X., and Xu, H. (2019). "Preparation of higher alcohols by biomass-based syngas from wheat straw over CoCuK/$ZrO_2$-$SiO_2$ catalyst," *Ind. Crop. Prod.* 131, 54-61. DOI: 10.1016/j.indcrop.2019.01.034

Guo, D., Song, X., Tan, L., Ma, H., Sun, W., Pang, H., Zhang, L., and Wang, X. (2019). "A facile dissolved and reassembled strategy towards sandwich-like rGO@NiCoAl-LDHs with excellent supercapacitor performance," *Chem. Eng. J.* 356, 955-963. DOI: 10.1016/j.cej.2018.09.101

He, Q.-Q., Wang, H.-Y., Lun, N., Qi, Y.-X., Liu, J.-R., Feng, J.-K., Qiu, J., and Bai, Y.-J. (2018). "Fabricating a $Mn_3O_4$/$Ni(OH)_2$ nanocomposite by water-boiling treatment for use in asymmetric supercapacitors as an electrode material," *ACS Sustain. Chem. Eng.* 6(11), 15688-15696. DOI: 10.1021/acssuschemeng.8b04195

Huang, J., Liang, Y., Dong, H., Hu, H., Yu, P., Peng, L., Zheng, M., Xiao, Y., and Liu, Y. (2018a). "Revealing contribution of pore size to high hydrogen storage capacity," *Int. J. Hydrogen Energ.* 43(39), 18077-18082. DOI: 10.1016/j.ijhydene.2018.08.027

Huang, S., Zhang, J., Li, P., Wang, W., Feng, H., and Luo, H. (2018b). "Preparation of metal-organic framework-derived nitrogen-doped porous carbon and study of its supercapacitive performance in potassium citrate electrolyte," *Appl. Surf. Sci.* 459, 120-128. DOI: 10.1016/j.apsusc.2018.07.140

Huang, Y., and Zhao, G. (2016). "Preparation and characterization of activated carbon fibers from liquefied wood by KOH activation," *Holzforschung* 70(3), 195-202. DOI: 10.1515/hf-2015-0051

Jeong, N., Kim, H.-K., Kim, W.-S., Choi, J. Y., Han, J.-H., Nam, J.-Y., Hwang, K.S., Yang, S., Jwa, E.-J., Kim, T.-Y., *et al.* (2019). "Uniform coating of molybdenum disulfide over porous carbon substrates and its electrochemical application," *Chem. Eng. J.* 356, 292-302. DOI: 10.1016/j.cej.2018.09.021

Kostoglou, N., Koczwara, C., Prehal, C., Terziyska, V., Babic, B., Matovic, B., Constantinides, G., Tampaxis, C., Charalambopoulou, G., Steriotis, T., *et al.* (2017). "Nanoporous activated carbon cloth as a versatile material for hydrogen adsorption, selective gas separation and electrochemical energy storage," *Nano Energy* 40, 49-64. DOI: 10.1016/j.nanoen.2017.07.056

Li, D., Li, W. B., Shi, J. S., and Xin, F. W. (2016). "Influence of doping nitrogen, sulfur, and phosphorus on activated carbons for gas adsorption of $H_2$, $CH_4$ and $CO_2$," *RSC Adv.* 6(55), 50138-50143. DOI: 10.1039/c6ra06620h

Lee, H.-M., Heo, Y.-J., An, K.-H., Jung, S.-C., Chung, D. C., Park, S.-J., and Kim, B.-J. (2017). "A study on optimal pore range for high pressure hydrogen storage behaviors by porous hard carbon," *Int. J. Hydrogen Energ.* 43(11), 5894-5902. DOI: 10.1016/j.ijhydene.2017.09.085

Ma, X. J., Zhang, F., Zhu, J. Y., Yu, L. L., and Liu, X. Y. (2014). "Preparation of highly developed mesoporous activated carbon fiber from liquefied wood using wood charcoal as additive and its adsorption of methylene blue from solution," *Bioresource Technol.* 164, 1-6. DOI: 10.1016/j.biortech.2014.04.050

Ramesh, T., Rajalakshmi, N., and Dhathathreyan, K. S. (2015). "Activated carbons

derived from tamarind seeds for hydrogen storage," *Journal of Energy Storage* 4, 89-95. DOI: 10.1016/j.est.2015.09.005

Rambau, K. M., Musyoka, N. M., Manyala, N., Ren, J., and Langmi, H. W. (2018). "Mechanochemical approach in the synthesis of activated carbons from waste tyres and its hydrogen storage applications," *Mater. Today: Proc*. 5, 10505-10513. DOI: 10.1016/j.matpr.2017.12.382

Sangeetha, D. N., and Selvakumar, M. (2018). "Active-defective activated carbon/$MoS_2$ composites for supercapacitor and hydrogen evolution reactions," *Appl. Surf. Sci.* 453, 132-140. DOI: 10.1016/j.apsusc.2018.05.033

Sawant, S. Y., Munusamy, K., Somani, R. S., John, M., Newalkar, B. L., and Bajaj, H. C. (2017). "Precursor suitability and pilot scale production of super activated carbon for greenhouse gas adsorption and fuel gas storage," *Chem. Eng. J.* 315, 415-425. DOI: 10.1016/j.cej.2017.01.037

Sethia, G., and Sayari, A. (2016). "Activated carbon with optimum pore size distribution for hydrogen storage," *Carbon* 99, 289-294. DOI: 10.1016/j.carbon.2015.12.032

Sevilla, M., and Mokaya, R. (2014). "Energy storage applications of activated carbons: Supercapacitors and hydrogen storage," *Energ. Environ. Sci.* 7(4), 1250-1280. DOI: 10.1039/c3ee43525c

Sreńscek-Nazzal, J., and Kiełbasa, K. (2019). "Advances in modification of commercial activated carbon for enhancement of $CO_2$ capture," *Appl. Surf. Sci*. 494, 137-151. DOI: 10.1016/j.apsusc.2019.07.108

Wróbel-Iwaniec, I., Díez, N., and Gryglewicz, G. (2015). "Chitosan-based highly activated carbons for hydrogen storage," *Int. J. Hydrogen Energ.* 40(17), 5788-5796. DOI: 10.1016/j.ijhydene.2015.03.034

Yang, F., Ren, J., Liu, Q., Zhang, L., Chai, Y., and Dai, W.-L. (2019). "Facile oxalic acid-assisted construction of laminated porous N-deficient graphitic carbon nitride: Highly efficient visible-light-driven hydrogen evolution photocatalyst," *Int. J. Hydrogen Energ.* 33, 1-8. DOI: 10.1016/j.jechem.2018.08.002

Zhou, L., Liu, D., Li, J., Tang, H., Xie, Z., and Qu, D. (2018). "Electrochemical hydrogen storage in a nitrogen-doped uniformed microporous carbon," *Int. J. Hydrogen Energ.* 43(31), 14096-14102. DOI: 10.1016/j.ijhydene.2018.06.029

Article submitted: May 14, 2019; Peer review completed: October 18, 2019; Revised version received: October 22, 2019; Accepted: October 23, 2019; Published: October 25, 2019.
DOI: 10.15376/biores.14.4.9755-9765